

UWB Radio Channel Modeling Considerations

J. Kunisch*

J. Pamp*

Abstract – In this work we try to approach the problem of UWB radio channel modeling from two different directions. At first, we consider basic properties of antennas, because they are essential elements of the radio channel. We present a self-contained description of the spatio-temporal transmit and receive characteristic for a generic antenna model. Based on that, general transfer function expressions for simple ideal UWB radio channels, in particular the free-space far-field channel and multipath channels, are given in terms of these characteristic functions. We then consider features of the UWB radio channel observable in measurement data, and finally draw some conclusions on UWB channel modeling.

1 INTRODUCTION

When going from wideband (WB) to ultra-wideband (UWB) radio channel modeling, a number of aspects have to be taken into account that amount to a changed overall behavior of the channel. In particular, the assessment of transmitted and received waveforms requires accurate and coherent models for each part of the channel. For example, a prominent phenomenon found for wideband channels is frequency selectivity which leads to dispersion of the transmitted signal. In many cases frequency selectivity can be attributed mainly to propagation effects (multipath) while dispersion effects introduced by the antennas may be less significant. For impulse radio applications, however, even the dispersive properties of antennas [2] have to be considered carefully.

By radio channel we understand the two-port or n -port formed by several antennas plus the corresponding propagation environment. Consequently, in the first part of the paper we address some issues related to antennas. In particular, we look into the spatio-temporal transmit and receive characteristic of the antennas and their relationship. Here, we present a self-contained formulation and derivation tailored to our purpose and partly based on the work of several authors [1][3][5][6][7]. The formulation is suited for antennas connected to a waveguide or transmission line. Based on these results, we give general transfer function expressions for the most simple free-space UWB radio channel and the ideal UWB multipath channel. We then move on to consider measured UWB radio channel data and discuss some of the apparent features different from those that are observed under typical wideband conditions and that are essential for proper UWB radio channel modeling.

In the following, rms phasors with an implied $\exp(j\omega t)$ time dependency are used, vectors are printed in bold typeface, unit vectors are denoted by a caret ($\hat{\mathbf{r}} \triangleq \mathbf{r}/\|\mathbf{r}\|$), and the tilde \sim denotes time dependent quantities.

2 ANTENNA PROPERTIES

In this section we introduce two characteristic functions \mathbf{A} and \mathbf{h} that describe the spatio-temporal transmission and reception characteristic of a generic antenna. These functions form the basis for general expressions for the UWB radio channel in Sec. 3.

2.1 Antenna Model

The antenna definition used here comprises two elements: (a) a material distribution $\varepsilon(\mathbf{r}, \omega)$, $\mu(\mathbf{r}, \omega)$ which differs from free space only within a finite volume, (b) a port defined by a reference plane on a waveguide (the antenna feed line). One part of the feed line up to the reference plane is considered part of the antenna. In the vicinity of the reference plane, the feed line is considered to be uniform such that at the reference plane power wave amplitudes a and b (corresponding to waves approaching and leaving the antenna, resp.) may be defined by

$$\begin{aligned} \mathbf{E}_{\text{tan}} &= \sum_n \sqrt{Z_n} \mathbf{e}_n(x, y) [a_n e^{-jk_n z} + b_n e^{+jk_n z}] \\ \mathbf{H}_{\text{tan}} &= \sum_n \sqrt{Y_n} \mathbf{h}_n(x, y) [a_n e^{-jk_n z} - b_n e^{+jk_n z}] \end{aligned} \quad (1)$$

where \mathbf{e}_n , \mathbf{h}_n , and $Z_n = 1/Y_n \in \mathbb{R}$ are the electric and magnetic fields tangential to the reference plane and feed line impedance for mode n , with $\mathbf{h}_n = \hat{\mathbf{z}} \times \mathbf{e}_n$ and normalization such that $\int_S \mathbf{e}_n \mathbf{e}_m = \delta_{m,n}$; the positive z -direction points towards the antenna. In the following, a single mode n is considered and for simplicity the index n is dropped. If necessary, corresponding results for several modes may be superimposed, as the modes on the considered feed line are orthogonal.

At the reference plane, the antenna acts as a source according to $b = b^i + \Gamma a$ with the source strength b^i evoked by an incident field and the output reflection coefficient Γ due to the antenna input impedance

* IMST GmbH, Carl-Friedrich-Gauß-Str. 2, 47475 Kamp-Lintfort, Germany
E-mail: {kunisch,pamp}@imst.de, Tel: +49 2842 981 454, Fax: +49 2842 981 499

Z_A , which in general is different from the feed line impedance Z ; a is the wave amplitude at the reference plane of the input signal used to excite transmission.

When transmitting, the electric far-field at \mathbf{r}_2 produced by an antenna at \mathbf{r}_1 may be given as

$$\mathbf{E}_1(\mathbf{r}_2, \omega) = \sqrt{Z_0} \frac{e^{-jk_0 r_{12}}}{\sqrt{4\pi r_{12}}} \mathbf{A}(\hat{\mathbf{r}}_{12}, \omega) a(\omega) \quad (2)$$

where $\mathbf{A}(\hat{\mathbf{r}}_{12}, \omega)$ is defined by (2) and represents the spatio-temporal transmit characteristic at angular frequency ω in direction $\hat{\mathbf{r}}_{12} \triangleq (\mathbf{r}_2 - \mathbf{r}_1) / \|\mathbf{r}_2 - \mathbf{r}_1\|$, and Z_0 is the free-space impedance. Under far-field condition, $\mathbf{A}(\hat{\mathbf{r}}_{12}, \omega) \perp \hat{\mathbf{r}}_{12}$. The dependence of $\mathbf{A}(\hat{\mathbf{r}}_{12}, \omega)$ on $\hat{\mathbf{r}}_{12}$ describes the radiation pattern and the dependence on ω describes the (temporal) transmission filter characteristics of the antenna. The power flux density corresponding to Eq. (2) is given by

$$S(\mathbf{r}_2) = \|\mathbf{E}_1(\mathbf{r}_2)\|^2 / Z_0 = \|\mathbf{A}(\hat{\mathbf{r}}_{12}, \omega)\|^2 |a|^2 / 4\pi r_{12}^2. \quad (3)$$

From the power $|a|^2$ approaching the antenna, only the amount $|a|^2(1 - |\Gamma|^2)$ actually enters into the antenna. Isotropic radiation of this power would produce a power flux density which on comparison with Eq. (3) gives the relation between \mathbf{A} and the gain over an isotropic antenna

$$G_{\text{iso}}(\hat{\mathbf{r}}_{12}, \omega) = \|\mathbf{A}(\hat{\mathbf{r}}_{12}, \omega)\|^2 / (1 - |\Gamma(\omega)|^2). \quad (4)$$

For the reception case, let

$$\mathbf{E}^i(\mathbf{r}, \hat{\mathbf{k}}, \omega) \triangleq \mathbf{E}^i(\hat{\mathbf{k}}, \omega) \exp(-jk_0 \hat{\mathbf{k}} \mathbf{r}),$$

be the electric field at position \mathbf{r} of an incident plane wave traveling into direction $\hat{\mathbf{k}}$, where $k_0 = \omega/c_0$ is the free-space wave number. The corresponding source strength b^i may be given as

$$b^i(\omega) = \sqrt{4\pi} \mathbf{h}(\hat{\mathbf{k}}, \omega) \mathbf{E}^i(\mathbf{r}, \hat{\mathbf{k}}, \omega) / \sqrt{Z_0}. \quad (5)$$

$\mathbf{h}(\hat{\mathbf{k}}, \omega)$ is defined by Eq. (5) and represents the spatio-temporal receive characteristic of the antenna under far-field (incident plane wave) conditions. Because $\mathbf{E}(\mathbf{r}, \hat{\mathbf{k}}) \perp \hat{\mathbf{k}}$ for plane waves, we additionally require $\mathbf{h}(\hat{\mathbf{k}}, \omega) \perp \hat{\mathbf{k}}$ to obtain a unique definition of \mathbf{h} . It should be noted that \mathbf{h} is defined with respect to the incident field, i.e., the field without the field

scattered at the antenna. Because \mathbf{h} linearly maps the electric field strength to the source strength b^i , \mathbf{h} acts like an effective length operator.

2.2 Transmit and Receive Characteristic Relation

Using the principle of reciprocity, it can be shown that the transmit and receive characteristics are related by (see Sec. 6.1 in the Appendix),

$$2j\omega \mathbf{h}(-\hat{\mathbf{k}}, \omega) = c_0 \mathbf{A}(\hat{\mathbf{k}}, \omega). \quad (6)$$

If Eq. (6) holds for all ω , the corresponding time domain expression

$$2(\partial/\partial t) \tilde{\mathbf{h}}(-\hat{\mathbf{k}}, t) = c_0 \tilde{\mathbf{A}}(\hat{\mathbf{k}}, t) \quad (7)$$

illustrates the well-known temporal derivative relation between transmit and receive impulse responses [1][3][4][7]. As will be seen below, this relation plays an important role in understanding basic properties of the UWB radio channel.

3 THE IDEAL FREE-SPACE FAR-FIELD UWB RADIO CHANNEL

This section gives expressions for the transfer function of the most simple UWB radio channel, i.e. the ideal free-space far-field UWB radio channel made up by two antennas in free-space and mutually in far-field. Single scattering is assumed, i.e. contributions that bounce back and forth between the two antennas are neglected. Furthermore, a generalized expression for the ideal multipath channel based on an extension of the free-space channel expression is given as well.

3.1 Transfer Function

For two antennas (designated by 1 and 2), and under the above given assumptions the transfer function

$$S_{21}(\omega) = \left. \frac{b_2}{a_1} \right|_{a_2=0} = \frac{b_2^i}{a_1}$$

of the corresponding ideal free-space far-field UWB radio channel may be given in various forms by combining Eqs. (2), (5), and (6) as

$$\begin{aligned} S_{21}(\omega) &= \mathbf{A}_1(\hat{\mathbf{r}}_{12}, \omega) \mathbf{h}_2(\hat{\mathbf{r}}_{12}, \omega) \frac{e^{-jk_0 r_{12}}}{r_{12}} \\ &= \mathbf{h}_1(\hat{\mathbf{r}}_{21}, \omega) \mathbf{A}_2(\hat{\mathbf{r}}_{21}, \omega) \frac{e^{-jk_0 r_{12}}}{r_{12}} \\ &= \frac{1}{j\omega} \frac{c_0}{2} \mathbf{A}_1(\hat{\mathbf{r}}_{12}, \omega) \mathbf{A}_2(\hat{\mathbf{r}}_{21}, \omega) \frac{e^{-jk_0 r_{12}}}{r_{12}} \\ &= j\omega \frac{2}{c_0} \mathbf{h}_1(\hat{\mathbf{r}}_{21}, \omega) \mathbf{h}_2(\hat{\mathbf{r}}_{12}, \omega) \frac{e^{-jk_0 r_{12}}}{r_{12}}. \end{aligned} \quad (8)$$

It is important to stress that the various vectors in Eq. (8) be referred to the same reference frame. In particular, if the orientation of an antenna changes with respect to that frame, the corresponding \mathbf{A} and \mathbf{h} will change. In the likely case that \mathbf{A} and \mathbf{h} are given with respect to an antenna fixed frame, the orientation of the antenna has to be accounted for by a proper transformation of \mathbf{A} and \mathbf{h} .

3.2 Extension to Multipath Conditions

If the transmission via a given path involves some intermediate interaction with the environment, the transfer function of that path may be modified to

$$S_{21}(\omega, \mathbf{r}_1, \mathbf{r}_2, \hat{\mathbf{k}}_D, \hat{\mathbf{k}}_A) = \mathbf{A}_1(\hat{\mathbf{k}}_D, \omega) \mathbf{h}_2(\hat{\mathbf{k}}_A, \omega) G(\omega, \mathbf{r}_1, \mathbf{r}_2, \hat{\mathbf{k}}_D, \hat{\mathbf{k}}_A) \quad (9)$$

where $\hat{\mathbf{k}}_D$ and $\hat{\mathbf{k}}_A$ are the directions of departing and incident waves, respectively. $G(\omega, \mathbf{r}_1, \mathbf{r}_2, \hat{\mathbf{k}}_D, \hat{\mathbf{k}}_A)$ is analogous to a scalar Green's function and describes the propagation part of the channel for reception at \mathbf{r}_2 (from direction $\hat{\mathbf{k}}_A$) when transmitting into direction $\hat{\mathbf{k}}_D$ at \mathbf{r}_1 . For example, for the ideal free-space far-field channel there is a non-zero

$$G(\omega, \mathbf{r}_1, \mathbf{r}_2, \hat{\mathbf{k}}_D, \hat{\mathbf{k}}_A) = \frac{e^{-jk_0 r_{12}}}{r_{12}}$$

only for $\hat{\mathbf{k}}_D = \hat{\mathbf{k}}_A = \hat{\mathbf{r}}_{12}$; and for a path containing an ideal specular reflection

$$G(\omega, \mathbf{r}_1, \mathbf{r}_2, \hat{\mathbf{k}}_D, \hat{\mathbf{k}}_A) = \frac{e^{-jk_0 r}}{r}$$

is non-zero if $\hat{\mathbf{k}}_D$ and $\hat{\mathbf{k}}_A$ are the directions to and from the mirror point, and r is the total path length. Generally, expressions for $G(\omega, \mathbf{r}_1, \mathbf{r}_2, \hat{\mathbf{k}}_D, \hat{\mathbf{k}}_A)$ may be derived e.g. by UTD.

Summing over all considered paths, and designating the l -th path with a superscript l , a general expression for the ideal UWB multipath channel transfer function is

$$S_{21}(\omega, \mathbf{r}_1, \mathbf{r}_2) = \sum_l \mathbf{A}_1^l(\hat{\mathbf{k}}_D^l, \omega) \mathbf{h}_2^l(\hat{\mathbf{k}}_A^l, \omega) G^l(\omega, \mathbf{r}_1, \mathbf{r}_2, \hat{\mathbf{k}}_D^l, \hat{\mathbf{k}}_A^l). \quad (10)$$

Like Eq. (8), Eqs. (9) and (10) can be cast into various forms.

3.3 Transition Wideband – Ultra-Wideband

In this section we discuss the implications of the previously given antenna properties and transfer

function expressions regarding the modeling of ultra-wideband channels and signals.

According to Eqs. (2) and (5), the antenna acts as a temporal filter. Let $s(\omega)$ denote the filter input signal, i.e., $a(\omega)$ for transmission and $\mathbf{E}^i(\omega)$ for reception, and let $r(\omega)$ denote the output signal, i.e., $\mathbf{E}_1(\omega)$ for transmission and $b^i(\omega)$ for reception.¹

It is evident from Eq. (6) that the transmission and reception filter characteristics are in general related by a factor $j\omega$. In other words, the distortion of the input waveform will be different in both directions. Now let $s(\omega)$ be band limited, i.e., non-zero only for $\omega \in B \triangleq \{\omega : |\omega| \in [\omega_c - \Omega/2, \omega_c + \Omega/2]\}$, $\omega_c, \Omega > 0$. For the reception case (denoted by superscript^R) we may then write Eq. (5) in the form

$$\tilde{r}^R(t) \propto \int_{\omega \in B} s^R(\omega) \mathbf{h}(\omega) \exp(j\omega t) d\omega, \quad (11)$$

and Eq. (2) for transmission (denoted by superscript^T)

$$\tilde{r}^T(t) \propto \int_{\omega \in B} s^T(\omega) \mathbf{A}(\omega) \exp(j\omega t) d\omega. \quad (12)$$

With Eq. (6), for transmission we also have

$$\begin{aligned} \tilde{r}^T(t) &\propto \int_{\omega \in B} s^T(\omega) j\omega \mathbf{h}(\omega) \exp(j\omega t) d\omega \\ &= \int_{\omega \in B} s^T(\omega) |\omega| \mathbf{h}(\omega) \exp(j\omega(t + \tau(\omega))) d\omega \end{aligned}$$

where $\tau(\omega) \triangleq \frac{\pi}{2|\omega|}$; the temporal derivative operator represented by $j\omega$ acts by frequency selective scaling (by a factor $|\omega|$) and shifting (by $\tau(\omega)$). In the (non-ultra-)wideband case we have $\Omega \ll \omega_c$; therefore approximations $|\omega| \approx \omega_c$, $\tau(\omega) \approx \pi/2\omega_c$ may be used to arrive at

$$\tilde{r}^T(t) \propto |\omega_c| \int_{\omega \in B} s^T(\omega) \mathbf{h}(\omega) \exp(j\omega(t + \tau(\omega_c))) d\omega. \quad (13)$$

By comparison of Eqs. (11) and (13), we find that, for $s^T(\omega) = s^R(\omega)$, in the wideband case approximately

$$r^T(t) \propto r^R\left(t + \frac{\pi}{2\omega_c}\right). \quad (14)$$

¹ To simplify notation, only the ω dependency is given explicitly here.

Therefore, in the wideband case, the antenna impulse responses in transmission and reception are approximately just shifted copies of each other. This is not the case under ultra-wideband conditions, where the full effect of the temporal derivative in expression (6) has to be taken into account for accurate waveform modeling, i.e., assuming again $s^T(\omega) = s^R(\omega)$,

$$\tilde{r}^T(t) \propto (\partial/\partial t)\tilde{r}^R(t) \quad (15)$$

Depending on the actual relative bandwidth Ω/ω_c , the relation between the transmit and receive filter characteristics may vary in between the extremes given by Eqs. (14) and (15).²

4 EMPIRICAL ASPECTS

In this section we change over to the experimental perspective on UWB channel modeling and consider UWB radio channel measurement data.

4.1 A Look at Measured Data

Figure 1 shows a typical average power delay profile (APDP) based on 30 x 30 baseband impulse responses $\tilde{S}_{21}(\mathbf{r}_1, \tau)$ taken on a 30 cm x 30 cm grid under LOS conditions in an office environment. The measurement band is 1-11 GHz, giving a nominal delay resolution of 100 ps (corresponding to 3 cm spatial resolution).³

Two global observations can be made here: First, the APDP is dominated by the LOS component arriving at about 8 ns, and for delays exceeding app. 30 ns, the APDP exhibits a single diffuse multipath (MP) cluster caused by superposition of a large number of unresolved paths. The MP cluster exhibits an exponential decay as function of the delay. The same type of behavior is commonly encountered under WB conditions. Second, in the delay range 8-30 ns, the MP cluster envelope deviates from a simple exponential decay behavior, and a number of strong echoes embedded in the surrounding MP components (MPC) can be clearly recognized. The high bandwidth of 10 GHz allows to resolve individual paths that correspond to specific interactions; by comparison with the geometry of the measurement environment, many of the strong echoes can be mapped to individual paths that undergo particular interactions including for example wall reflections, ceiling-wall reflections etc.

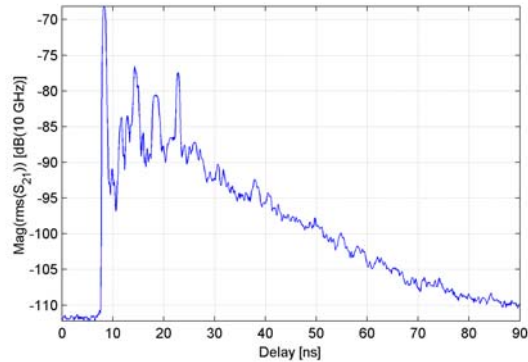


Figure 1: Example for UWB average power delay profile.

In the same delay range, the envelope of the diffuse MP cluster starts from lower values and increases up to the delay value of about 20-30 ns, which roughly marks the onset of the diffuse MPC regime. This behavior results from the fact that for the existence of diffuse MP a large number of paths are required to superimpose. For short delay values, however, the available number of paths that have the corresponding short excess delay is too low, because the average distance to scatterers is much larger than the delay resolution. Note that for a lower measurement bandwidth, the energy contained in the individual echoes would be spread out over a larger delay range, thus giving rise to an MPC cluster envelope that would exhibit a (not necessarily) exponential decay characteristic starting from excess delay 0, i.e., from the LOS arrival.

Figure 2 shows color-coded power delay profiles for 150 impulse responses. These responses were obtained by displacing the Tx antenna along a straight line of 150 cm length such that the direction of movement was roughly perpendicular to the Rx-Tx direction; the distance between Rx and Tx was approximately 3 m. According to the direction of movement the delay of various MPCs changes. In particular, the delay of the LOS component changes from app. 11 ns at the beginning to app. 9 ns at the end of the 150 cm long straight line. It is possible to recognize a slight curvature (convex if viewed from the left hand side) that accurately reflects the geometry of the setting. From Figure 2 it is even recognizable that at the end of the 150 cm movement the nearest point along the line of movement (the point of shortest Tx-Rx separation) was not yet reached.

There are some more traces recognizable that are parallel to the LOS trace, i.e., they show the same delay versus displacement tendency. This suggests that these traces correspond to paths that belong to

² For a truly narrowband signal $\tilde{r}^R(t) = \cos(\omega_c t + \phi)$, Eqs. (14) and (15) are equivalent due to $(\partial/\partial t)\tilde{r}^R(t) \propto r^R(t + (\pi/2\omega_c))$

³ A more detailed description of the underlying measurement data and environments is given in [8].

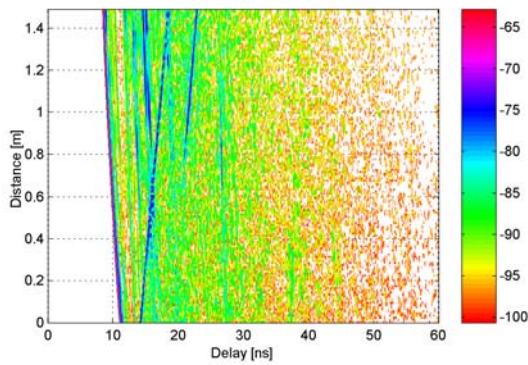


Figure 2: Color-coded power delay profiles for 150 baseband impulse responses along 150 cm of Tx displacement almost perpendicular to the Rx-Tx line of sight.

the same vertical plane that contains Rx and Tx and the LOS path. In fact, by comparison with the geometry of the room, some of these traces can be associated with the paths traveling via floor and ceiling.

In Figure 2 another group of parallel traces can be recognized that exhibit increasing delay as the antenna moves (from bottom to top). While the Tx antenna is slightly approaching the Rx antenna due to the movement, thus causing a decrease in delay for the LOS trace, these traces correspond to scatterers from which the antenna is moving away. Again, from geometry, the strongest echo of this group corresponds to a path leading from Tx via a wall to Rx. Unlike the LOS trace, this trace does not exhibit a significant curvature within the accuracy limits of the plot.

Assuming that the wall reflection itself does not introduce any appreciable (group) delay, observed delays can be mapped to geometrical path lengths. In this case, the delay values of the LOS trace and the trace of the wall reflected path provide range estimates for two receiver positions, namely the actual position of the receiver, and the position of its image. By using the knowledge of the room geometry and receiver position, an estimate of the Tx position could be given based solely on the traces from Figure 2.⁴ Furthermore, using the same information, the statement given above that the “direction of movement was roughly perpendicular to the Rx-Tx direction” could be refined to give the actual angle between direction of movement and Tx-Rx direction.

If the wall reflection in fact would cause a non-negligible delay, the delay values actually provide pseudo-ranges that, by means of a model of the wall reflection, could in principle be corrected.

⁴ Actually, with just two ranges, one additional constraint for the unknown position is required, e.g. the height.

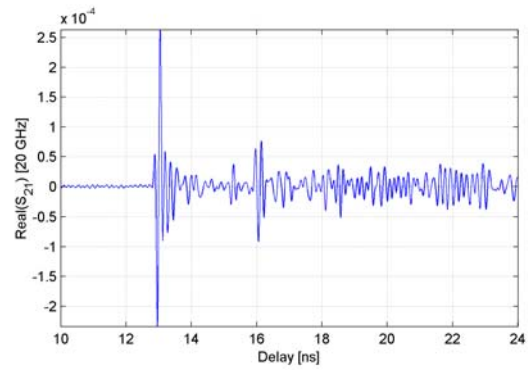


Figure 3: Example for a single measured UWB impulse response in passband. A Kaiser-Bessel frequency domain window has been applied.

Actually, as far as such global geometry considerations are concerned, the channel behavior is in principle scalable regarding distances and bandwidths, and plots that are similar to Figure 2 have been obtained for years by certain outdoor measurements.

A very simple, but nevertheless distinguishing feature of UWB is that these resolution capabilities are made available at room scale.

It is obvious that a channel model suitable e.g. for positioning applications necessarily has to consider these essential UWB channel features.

At some points in the plot, several traces intersect each other. In these regions a regular fading pattern is clearly recognizable that, unlike what is observable in the WB case, nicely illustrates the result of the superposition of just two individual paths.

Figure 3 shows an example for a single measured UWB impulse response (IR). While the previous examples employed equivalent baseband representations, the IR in Figure 3 is shown in passband, i.e., the real valued signal as it would be measured e.g. by a DSO. As the measurement was actually band limited (1-11 GHz) and VNA based, a frequency domain window was applied to suppress side lobes. In particular, a Kaiser-Bessel window was employed. Thus, in effect, Figure 3 shows the response of the channel to an impulse that equals the impulse response of the frequency domain window. Some strong echoes are visible, as before, as well as some ringing around these strong echoes. At about 10 ns of excess delay (corresponding to 3 m excess path length), individual echoes are hardly anymore recognizable.

Figure 4 shows two examples for averaged transfer functions. A frequency decay is clearly recognizable. A comparison with Eq. (8) (third line) suggests that the transmit characteristic \mathbf{A} of the employed antennas is reasonably flat over the considered band.

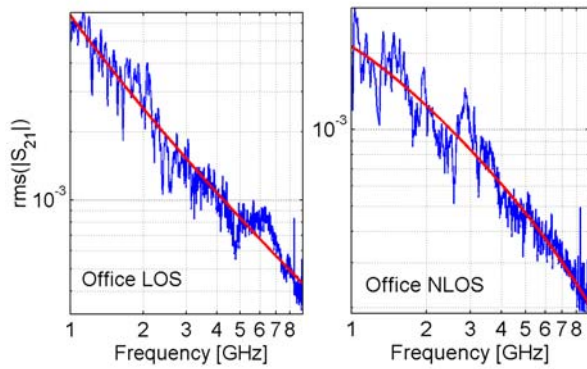


Figure 4: Example for rms average of 30 x 30 transfers functions for Office environment. LOS (left) and NLOS (right) conditions.

4.2 Implications on UWB Channel Modeling

As was demonstrated by some examples, the measurement data exhibit distinguishing features of the UWB radio channel that, unlike the WB case, need additional treatment.

The increased bandwidth allows to resolve individual paths that correspond to certain interactions with the environment. The main characteristic of these paths is that they are composed of very few, if not a single, components. Nevertheless, even under UWB conditions there is still an appreciable amount of diffuse, irresolvable multipath components that contribute a considerable part of the signal energy. Therefore, models that consist solely of a few sparsely distributed echoes miss essential aspects of the UWB channel. Many UWB typical applications rely on the existence of highly resolvable strong individual echoes. For a realistic performance assessment it is essential for the channel model to represent those influences that degrade the accuracy of the detection and estimation of these strong echoes. Apart from dense multipath components, there are also limitations imposed on resolvability imposed by the antennas.

A simple litmus test for the achievability of a particular resolution accuracy with a given UWB channel consists of the comparison of impulse responses extracted from partial bands at opposite ends of the band under consideration. The achievable overall accuracy (as opposed to nominal resolution) is not expected to exceed the accuracy limits recognizable by apparent differences in these sub-band impulse responses.

For the analysis of moving terminals, the modeling of Doppler behavior is required. Regarding dense multipath components, due to their very nature as superposition of a large number of components, methods well known for WB channels can be employed.

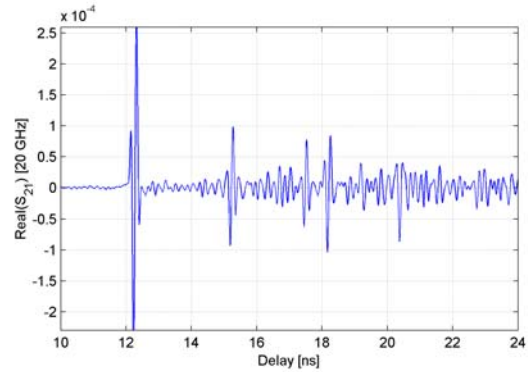


Figure 5: Example for a single modeled UWB impulse response (initial 10 ns of excess delay, passband). A Kaiser-Bessel frequency domain window has been applied.

Regarding individual components, the observed properties suggest to employ a more deterministic type of modeling approach corresponding to the less erratic spatial characteristics of these echoes

The authors have proposed a UWB radio channel indoor model along these lines for WPAN applications [9]. An example for a modeled impulse response is shown in Figure 5

5 CONCLUSIONS

General expressions for transfer functions of the ideal free-space and multipath UWB radio channel have been given based on transmit and receive characteristic functions for antennas and their relation presented in Sec. 2. This relation implies that for low relative bandwidth (WB case) the impulse responses of an antenna in transmission and reception tend to be similar up to a time shift while for large relative bandwidths (UWB) both impulse responses are related by the familiar temporal derivative relationship.

An inspection of measurement data reveals that the UWB channel exhibits both differences and commonalities to the wideband channel. A particularly significant difference is the occurrence of some individually resolvable echoes corresponding to single paths. These paths exhibit smooth variations when an antenna is moved, as opposed to dense multipath. Common to both channels is the occurrence of dense multipath. The onset of the dense multipath regime is shifted towards larger delays in the UWB case, while for lower delay values the energy tends to be more concentrated in individual echoes.

Acknowledgements

The authors are most grateful to Christophe Roblin (ENSTA, France) for his essential support in obtaining reference [1].

6 APPENDIX

6.1 Derivation of Transmit-Receive Relation

If two solutions $(\mathbf{E}_a, \mathbf{H}_a, \mathbf{J}_a, \mathbf{K}_a)$ and $(\mathbf{E}_b, \mathbf{H}_b, \mathbf{J}_b, \mathbf{K}_b)$ of Maxwell's curl equations

$$\begin{aligned} \nabla \times \mathbf{E} + j\omega\mu\mathbf{H} &= -\mathbf{K} \\ -\nabla \times \mathbf{H} + j\omega\varepsilon\mathbf{E} &= -\mathbf{J} \end{aligned} \quad (16)$$

pertain to the same material distribution within a volume V (and possibly different materials outside), then these solutions are subject to the Lorentz reciprocity constraint [4]

$$\oint_{\partial V} (\mathbf{E}_a \times \mathbf{H}_b - \mathbf{E}_b \times \mathbf{H}_a) \hat{\mathbf{n}} = \int_V (\mathbf{J}_a \mathbf{E}_b - \mathbf{K}_a \mathbf{H}_b) - (\mathbf{J}_b \mathbf{E}_a - \mathbf{K}_b \mathbf{H}_a). \quad (17)$$

Two such solutions are constructed as follows.

Solution (a) We consider an antenna at position \mathbf{r}_1 embedded in free space. In the reference plane of the antenna port, electric and magnetic surface current densities

$$\begin{aligned} \mathbf{J}_A &= \hat{\mathbf{z}} \times \mathbf{h}_n \sqrt{Y} a \\ \mathbf{K}_A &= \mathbf{e}_n \times \hat{\mathbf{z}} \sqrt{Z} a \end{aligned} \quad (18)$$

are impressed to excite the field of mode n traveling into the antenna with amplitude a . Due to this source arrangement, no fields are excited on the other side of the reference plane. Effectively, these surface current densities constitute an ideal wave source for mode n and amplitude a connected to the input port of the antenna. The transmitted field at a point \mathbf{r}_2 is given by Eq. (2).

Solution (b) No current densities are impressed at the antenna port. An elementary electric dipole, i.e., an electric current density

$$\mathbf{J}_2 = I_2 l \delta^3(\mathbf{r} - \mathbf{r}_2) \hat{\mathbf{v}}$$

is impressed at position \mathbf{r}_2 (same as for solution (a)) in the *presence* of the antenna at \mathbf{r}_1 , leading to a total field

$$\mathbf{E}_2(\mathbf{r}) = \mathbf{E}_2^i(\mathbf{r}, \hat{\mathbf{r}}_{21}) + \mathbf{E}_2^s(\mathbf{r}, \hat{\mathbf{r}}_{21}, \mathbf{E}_2^i) \quad \text{where} \\ \mathbf{E}_2^s(\mathbf{r}, \hat{\mathbf{r}}_{21}, \mathbf{E}_2^i) \text{ is the field scattered at the antenna.}$$

Result The result (6) is obtained by inserting the above constructed solutions into the reciprocity relation Eq. (17), letting $V = \mathbb{R}^3$ and considering that according to the definition of \mathbf{h} in Eq. (5) the antenna source strength b^i depends only on the *inci-*

dent field, i.e., the field the elementary electric dipole would produce in *absence* of the antenna,

$$\mathbf{E}_2^i(\mathbf{r}_1, \hat{\mathbf{r}}_{21}) = -j\omega\mu_0 \frac{e^{-jk_0 r_{21}}}{4\pi r_{21}} I_2 l (\hat{\mathbf{v}} - \hat{\mathbf{r}}_{21} (\hat{\mathbf{r}}_{21} \hat{\mathbf{v}}));$$

and furthermore considering that the orientation $\hat{\mathbf{v}}$ of the elementary dipole can be chosen arbitrarily.

6.2 Other Formulations

The received wave b^i corresponds to a voltage wave leaving the antenna with amplitude $U^- = \sqrt{Z} b^i$. Introducing

$$\mathbf{h}_N(\hat{\mathbf{k}}, \omega) \triangleq \sqrt{4\pi} \mathbf{h}(\hat{\mathbf{k}}, \omega), \quad (19)$$

the receive relationship Eq. (5) may be written in the form

$$\frac{U^-(\omega)}{\sqrt{Z}} = \mathbf{h}_N(\hat{\mathbf{k}}, \omega) \frac{\mathbf{E}_2^i(\mathbf{r}_1, \hat{\mathbf{k}}, \omega)}{\sqrt{Z_0}}$$

and, in time domain,

$$\frac{U^-(t)}{\sqrt{Z}} = \tilde{\mathbf{h}}_N(\hat{\mathbf{k}}, t) * \frac{\tilde{\mathbf{E}}_2^i(\mathbf{r}_1, \hat{\mathbf{k}}, t)}{\sqrt{Z_0}} \quad (20)$$

where $*$ denotes convolution.

Similarly, considering that an input wave a corresponds to a voltage wave with amplitude $U^+ = \sqrt{Z} a$ approaching the antenna, from Eqs. (2), (6), and (19) we get

$$\frac{\mathbf{E}_1(\mathbf{r}_2, \omega)}{\sqrt{Z_0}} = \frac{e^{-jk_0 r_{12}}}{2\pi c_0 r_{12}} j\omega \mathbf{h}_N(-\hat{\mathbf{r}}_{12}, \omega) \frac{U^+(\omega)}{\sqrt{Z}}, \quad (21)$$

with various forms of the time domain equivalent

$$\begin{aligned} \frac{\tilde{\mathbf{E}}_1(\mathbf{r}_2, t + r_{12}/c_0)}{\sqrt{Z_0}} &= \frac{1}{2\pi c_0} \frac{1}{r_{12}} \frac{\partial}{\partial t} \left(\tilde{\mathbf{h}}_N(-\hat{\mathbf{r}}_{12}, t) * \frac{U^+(t)}{\sqrt{Z}} \right) \\ &= \frac{1}{2\pi c_0} \frac{1}{r_{12}} \left(\frac{\partial}{\partial t} \tilde{\mathbf{h}}_N(-\hat{\mathbf{r}}_{12}, t) \right) * \frac{U^+(t)}{\sqrt{Z}} \\ &= \frac{1}{2\pi c_0} \frac{1}{r_{12}} \tilde{\mathbf{h}}_N(-\hat{\mathbf{r}}_{12}, t) * \frac{\partial U^+(t)}{\partial t} \frac{1}{\sqrt{Z}}. \end{aligned} \quad (22)$$

Eqs. (20) and (22) express both the transmit and receive characteristic by means of a single effective height operator \mathbf{h}_N . These equations correspond to those given in [7].

Note that the last form of the transmission equation (22) seems to suggest that the input signal is *always* differentiated before being transmitted.

Alternatively, however, instead of using a single effective height \mathbf{h}_N , we may introduce a renormalized gain characteristic

$$\mathbf{A}_N(\hat{\mathbf{r}}_{12}, \omega) \triangleq \mathbf{A}(\hat{\mathbf{r}}_{12}, \omega) / \sqrt{4\pi}; \quad (23)$$

then, from Eqs. (2), (5), (6), and (23)

$$\begin{aligned} \frac{U^-(t)}{\sqrt{Z}} &= 2\pi c_0 \int \tilde{\mathbf{A}}_N(-\hat{\mathbf{k}}, t) * \frac{\tilde{\mathbf{E}}_2(\mathbf{r}_1, \hat{\mathbf{k}}, t)}{\sqrt{Z_0}} dt \\ &= 2\pi c_0 \tilde{\mathbf{A}}_N(-\hat{\mathbf{k}}, t) * \int \frac{\tilde{\mathbf{E}}_2(\mathbf{r}_1, \hat{\mathbf{k}}, t)}{\sqrt{Z_0}} dt \end{aligned} \quad (24)$$

and

$$\frac{\tilde{\mathbf{E}}_1(\mathbf{r}_2, t + r_{12}/c_0)}{\sqrt{Z_0}} = \frac{1}{r_{12}} \tilde{\mathbf{A}}_N(\hat{\mathbf{r}}_{12}, t) * \frac{U^+(t)}{\sqrt{Z}} \quad (25)$$

Transmission equation (25) is equivalent to Eq. (22) and seems to suggest that the input signal is *never* differentiated before being transmitted.

This is only an apparent contradiction because the output signal depends on *two* factors: the input signal and the impulse response (\mathbf{h}_N or \mathbf{A}_N). In general, \mathbf{h}_N or \mathbf{A}_N can introduce any filter characteristic (within constraint (6)).

However, a few general statements regarding operations that are always or never performed on the input signal by an antenna can be made. For example, despite the apparent proportionality of radiated field and input voltage in Eq. (25), radiation at $\omega = 0$ is always impeded because $\mathbf{A}(\omega = 0) = 0$ due to Eq. (6) for finite $\mathbf{h}(\omega = 0)$.

6.3 Relation to Standard Antenna Parameters

In this section we give a few common antenna parameters in terms of the transmit and receive characteristic functions \mathbf{A} and \mathbf{h} .

The power available from the receiving antenna is given by

$$P_{av} = \frac{|b^i|^2}{1-|\Gamma|^2} = \frac{4\pi \|\mathbf{h}(\hat{\mathbf{k}})\|^2 \|\mathbf{E}^i(\mathbf{r}_1, \hat{\mathbf{k}})\|^2}{1-|\Gamma|^2 Z_0}$$

where matching polarization states are assumed.

Hence, the effective area for reception of a plane wave incident from direction $\hat{\mathbf{k}}$ is given by (using Eqs. (6) and (4))

$$A_{eff}(\hat{\mathbf{k}}) = \frac{4\pi \|\mathbf{h}(\hat{\mathbf{k}})\|^2}{1-|\Gamma|^2} = \frac{\lambda^2 \|\mathbf{A}(-\hat{\mathbf{k}})\|^2}{4\pi (1-|\Gamma|^2)} = \frac{\lambda^2}{4\pi} G_{iso}(-\hat{\mathbf{k}}).$$

If the antenna port is terminated with an ideal open circuit (reflection coefficient 1), the open circuit voltage is given by

$$U^{o.c.} = \sqrt{Z} \frac{2}{1-\Gamma} b^i = \sqrt{Z} \frac{4\sqrt{\pi}}{1-\Gamma} \mathbf{h} \frac{\mathbf{E}^i}{\sqrt{Z_0}} \triangleq \mathbf{h}_{eff} \mathbf{E}^i.$$

From that, the effective length follows as

$$\mathbf{h}_{eff} = \frac{4\sqrt{\pi}}{1-\Gamma} \sqrt{\frac{Z}{Z_0}} \mathbf{h}.$$

References

- [1] Deschamps, G. A., "I – Le Principe de Réciprocité en Electromagnétisme; II – Application du Principe de Réciprocité aux Antennas et aux Guides d'Ondes", *Revue du Cethedec* no 8, pp. 71-101, 1966
- [2] Schmitt, H. J. et al., "Calculated and Experimental Response of Thin Cylindrical Antennas to Pulse Excitation," *IEEE Trans. Antennas Propagat.*, vol. AP-14, No. 2, March 1966
- [3] Kanda, M., "Time Domain Sensors for Radiated Impulsive Measurements," *IEEE Trans. Antennas Propagat.*, vol. AP-31, No. 3, May 1983
- [4] Lo, Y.T., Lee, S.W., (Eds.) *Antenna Handbook*, Chapter 2 "Theorems and Formulas," Van Nostrand Reinhold, 1988
- [5] Baum, C., "General Properties of Antennas," *Sensor and Simulation Note 330*, 1991
- [6] Shlivinski, A. et al., "Antenna Characterization in the Time Domain," *IEEE Trans. Antennas Propagat.*, vol. AP-45, No. 7, July 1997
- [7] Farr, E. G., Baum, C., "Time Domain Characterization of Antennas with TEM Feeds," *Sensor and Simulation Note 426*, 1998
- [8] J. Kunisch, J. Pamp, "Measurement Results and Modeling Aspects for the UWB Radio Channel," *Proceedings IEEE UWBST 2002 Conference*, May 2002
- [9] J. Kunisch, J. Pamp, "Radio Channel Model for Indoor UWB WPAN Environments," *IEEE 802.15 document P802.15-02/281*, 2002.